Strength of silicon containing nanoscale flaws

Antonia Pajares,[a] Marina Chumakov,[b] and Brian R. Lawn[c]
Materials Science and Engineering Laboratory, National Institute of Standards and Technology, Gaithersburg, Maryland 20899-8500

(Received 21 August 2003; accepted 18 November 2003)

Silicon is a principal material in submicrometer-scale devices. Components in such devices are subject to intense local stress concentrations from nanoscale contacts during function. Questions arise as to the fundamental nature and extent of any strength-degrading damage incurred at such contacts on otherwise pristine surfaces. Here, a simple bilayer test procedure is adapted to probe the strengths of selected areas of silicon surfaces after nanoindentation with a Berkovich diamond. Analogous tests on silicate glass surfaces are used as a control. The strengths increase with diminishing contact penetration in both materials, even below thresholds for visible cracking at the impression corners. However, the strength levels in the subthreshold region are much lower in the silicon, indicating exceptionally high brittleness and vulnerability to small-scale damage in this material. The results have important implications in the design of devices with silicon components.

With the ever-increasing miniaturization of micro- and nanoelectromechanical systems (MEMS and NEMS), computer chips, sensors, hard drives, and other small-scale devices, materials reliability is a critical factor.[1,2] This is especially true of silicon, the material of choice for a large range of such devices. Characteristic dimensions associated with intercomponent contacts, surface asperities, and so forth, tend to scale down with device size. A key issue is whether basic strength relations at the macroscale extrapolate down below the microscale. Strength studies have been carried out on lithographically fabricated small-scale silicon specimens with near-pristine surfaces representative of MEMS components.[3,4] Uncommonly high strengths are typical, in the GPa range, but data interpretation in relation to initiating flaws tends to be speculative—the possibility that flaw characteristics may fundamentally change with diminishing scale is rarely considered. Hence the larger question—what is the nature of strength-governing, nanoscale flaws in silicon and other brittle materials?

Strength studies on surfaces of newly fabricated specimens are not always pertinent to real applications because lifetime-limiting flaws may develop during subsequent function. History-dependent degradation of initially pristine optical glass fibers is a well-documented example—a single contact of a pristine surface by an errant hard particle or asperity may diminish strength by over an order of magnitude.[5] Small-scale devices with moving components are especially susceptible to such contacts. Even low loads can induce inordinately high local stresses, exceeding theoretical cohesive bond limits, if the contact area is sufficiently small.

In the current study, a nanoindenter is used to simulate small-scale contacts in silicon. Nanoindentation produces flaws whose characteristic dimensions (e.g., indenter penetration h) are controlled by contact load (normal force P), enabling systematic study over a wide size range. A primary feature of contact flaws in brittle materials is that there tends to exist a threshold scale, typically 1 μm, below which cracking around the indentation site becomes suppressed,[6] suggesting immediately that extrapolations into the small-scale region need to be made with extreme caution. Interestingly, as has been demonstrated in earlier studies on pristine silicate glass fibers and rods,[7–11] even subthreshold contacts can degrade the strength of brittle materials. The aim of this study is to use the nanoindentation approach to establish a basis for quantifying any such strength degradation for silicon and, ultimately, other potential device materials.

[a]On leave from Departamento de Física, Facultad de Ciencias, Universidad de Extremadura, 06071 Badajoz, Spain.
[b]Undergraduate student, Department of Materials Science and Engineering, Lehigh University, Bethlehem, PA 18015.
[c]Address all correspondence to this author.
e-mail: brian.lawn@nist.gov

Silicon wafers (University Wafer, South Boston, MA) with highly polished (100) surfaces (<1 nm surface finish) were cut into plates 25 × 25 × 1 mm, taking care to protect the surfaces from spurious damage. For comparative control tests, soda-lime glass plates were cut to similar dimensions from microscope slides (Fisher Scientific, Pittsburgh, PA) and surface-etched (10 vol% HF for 9 min) to remove handling defects. Nanoindentations (Nanoindenter XP, MTS Systems Corp., Oak Ridge, TN) were made at the plate centers using a Berkovich indenter (tip radius <100 nm) with one edge aligned along the [010] direction in the case of silicon, in air. Load displacement (P–h) functions were recorded for each indentation. The indentation sites were examined for cracking using atomic force microscopy (AFM).

Strengths of the indented plates were measured using a simple bilayer test configuration.[12,13] The indented plates were bonded with a thin layer of epoxy (~10 μm) to a polycarbonate base 12.5 mm thick, with the indentation surface face down. Some plates were bonded without preindentation. The bilayers were then centrally loaded at their top surfaces with a sphere using a mechanical testing machine (Instron 8500, Instron Corp., Boston, MA), thus placing the plates in a state of flexure on the compliant support base. This specimen configuration was chosen because the zone of tension at the plate underface is confined to a small central area about the load axis,[14] thus minimizing premature failures from occasional larger defects, edge flaws, and specimen supports. A camera system located immediately below a small hole in the specimen stage facilitated accurate alignment of the indentation sites along the load axis.[12] In situ observations during testing enabled direct determination of the critical loads (L) at which failure initiated from an indentation flaw. Equivalent strengths (S) were calculated using the bilayer relation $S = (L/Bd^2)\log(E/E_s)$, where d is the plate thickness, E/E_s is the plate/substrate modulus ratio, and $B = 1.35$.[15]

Strengths S as a function of peak indentation load P (lower axis) or indenter penetration h (upper axis) are shown in Fig. 1 for soda-lime glass and in Fig. 2 for silicon. These figures include AFM images of indentation sites at selected loads for the two materials. The strength data cover more than four orders of magnitude in P and two in h. Filled symbols indicate the present Berkovich data. Unfilled symbols represent data from previous studies on glass[9,11] and silicon,[16] albeit for somewhat different material surfaces, indenters, and environment conditions. With due allowance for systematic shifts attributable to variations in test conditions, the data for the current and earlier studies follow similar trends. Vertical dashed lines indicate indentation conditions above which radial cracks are seen at the indentation corners and below which radial cracks are suppressed. Solid lines are simple fits through the data, according to

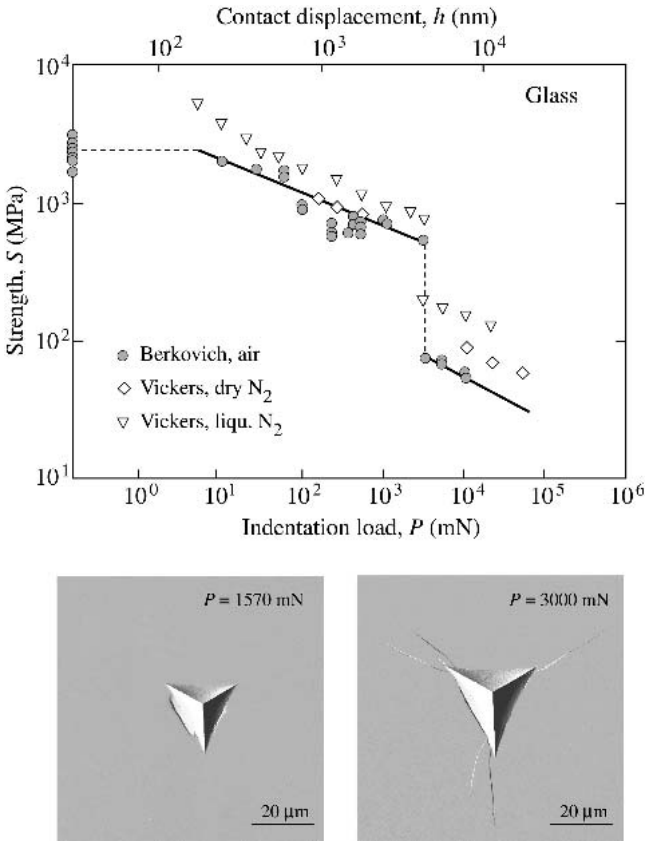

FIG. 1. Strength S of soda-lime glass plates as a function of indentation load P (lower axis) and penetration h (upper axis). Filled symbols are current bilayer data for Berkovich indentations (air tests). Unfilled symbols are flexure data from previous studies—Vickers indentations on glass rods (dry N_2 gas)[9] and on optical fibers (liquid N_2).[11] Data on left axis are from surfaces without indentations. Solid lines are data fits. Vertical dashed line delineates threshold for radial cracking; horizontal dashed line indicates strength of unindented surfaces. Micrographs are AFM images of Berkovich indentations either side of radial cracking threshold.

the well-established relation $S \propto P^{-1/3}$ in the postthreshold region[17] and with arbitrary slope in the subthreshold region. The data are limited at high loads by severe chipping around the indentations[18] and at low loads by naturally occurring surface flaws (horizontal dashed line).

To enable a direct comparison between the two materials, the lines from Figs. 1 and 2 are plotted on a common S–h diagram in Fig. 3. Both materials show increasing strength with diminishing indentation flaw size h, extending well into the GPa region. However, there are notable differences between the two materials. In the postthreshold region, the strengths are comparable at any given indenter penetration. In the subthreshold region, the silicon is substantially weaker than the glass, by as much as a factor of 5. In addition, the transition from postthreshold to subthreshold is continuous in the silicon, but abrupt in the glass. The abruptness in the latter case

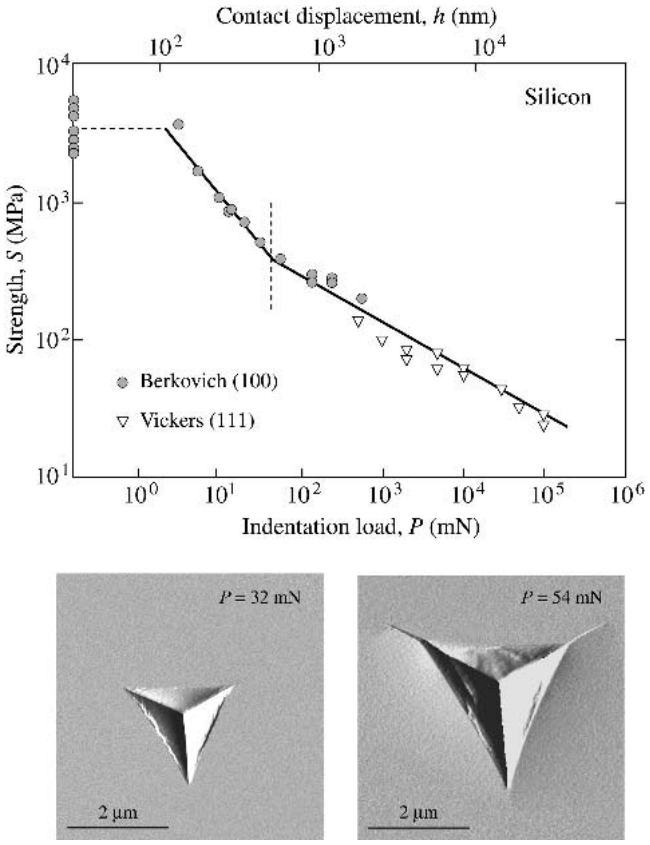

FIG. 2. Strength S of silicon (100) plates as a function of indentation load P (lower axis) and penetration h (upper axis). Filled symbols are current bilayer data for Berkovich indentations (air tests). Unfilled symbols are flexure data from previous studies in postthreshold region, Vickers indentations on silicon (111) plates.[16] Data on left axis are from surfaces without indentations. Solid lines are data fits. Vertical dashed line delineates threshold for radial cracking; horizontal dashed line indicates strength of unindented surfaces. Micrographs are AFM images of Berkovich indentations either side of radial cracking threshold.

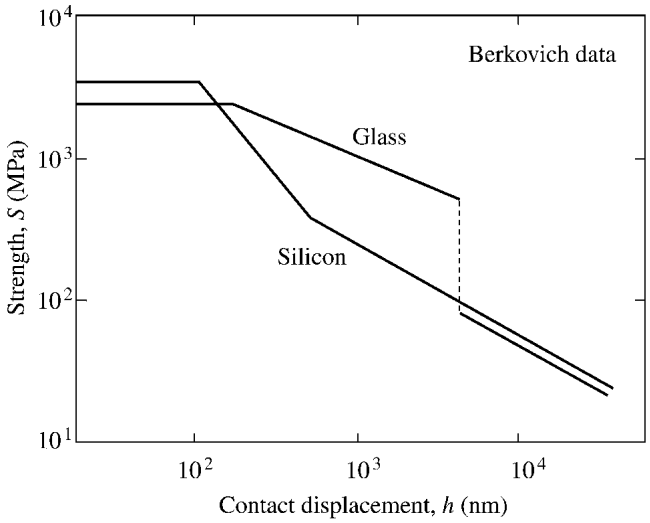

FIG. 3. Composite plot of S–h data, solid lines from Figs. 1 and 2. Note that silicon has superior strength in postthreshold contact region but inferior strength in subthreshold region.

is reflected somewhat by the relatively large radial crack size in the immediate postthreshold region for glass (compare micrographs in Figs. 1 and 2). Thus, the silicon has a much lower threshold for cracking and is accordingly much more vulnerable to strength-degrading damage from nanometer-scale contacts. In neither material is simple extrapolation from the macroscale to the nanoscale valid, although any such extrapolation might be used as a basis for lower-bound predictions (conservative design).

Micromechanical models accounting for the kinds of transitions in strength response described here have been outlined in the indentation literature.[9–11,19] Such models can be complex, and only the essential features will be described here. The source of radial cracking has been identified from optical and scanning electron microscopy as precursor slip bands or shear faults that constitute the plastic hardness zone.[9,20–23] The shear faults tend to be discrete and abrupt, occurring at stresses approaching the theoretical cohesive shear strength. The shear faults tend to follow crystallographic weak planes in single crystals and trajectories of maximum shear stress in glass. Above a critical indenter penetration, radial cracks nucleate from stress concentrations at intersections between mutually inclined slip bands. Figure 4 illustrates schematically how the slip process accommodates the high strains beneath the penetrating indenter and subsequently initiates the crack. The schematic represents a view along a diagonal of the Berkovich indenter and shows subsurface traces of the slip and crack planes. The crack has a penny-like geometry and extends to the top surface to form the characteristic radial traces seen in Figs. 1 and

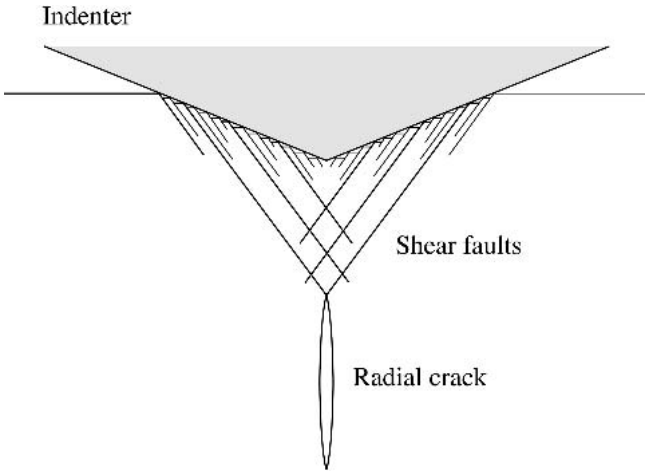

FIG. 4. Schematic of shear fault formation accommodating penetration h of indenter at load P. View is along an indentation half-diagonal. At threshold contact size, stress concentrations at intersecting shear fault surfaces initiate cracks that extend to the top surface to produce the radial arms viewed in Figs. 1 and 2.

2.[24] Recent studies of cross sections through small-scale indentations by transmission electron microscopy have verified this mechanism in silicon and other semiconductor single crystals.[25–27] The stress intensification at intersecting shear faults persists after contact is complete, so even subthreshold flaws remain effective sources of failure. The magnitude of the stress intensification is governed by the scale of the slip bands, in turn governed by the penentration h, accounting for the continuing strength degradation in the subthreshold regions of Figs. 1 and 2.[9] This essential two-step, slip–fracture process means that the strength characteristics in the subthreshold region are ultimately determined by material hardness as well as toughness.[19,28] A more detailed description of the material aspects of the micromechanical modeling, with an account of the relative differences in behavior between silicon, glass, and other brittle materials, as well as potential effects of surface states (e.g., polished, etched, oxidized) and slow crack growth will be pursued elsewhere.

Conclusions may be summarized thus: (i) simple strength testing of materials containing controlled nanocontact flaws can be used to simulate and quantify susceptibility to small-scale contacts; (ii) there is a subthreshold contact region where attendant cracking is no longer apparent, but where failure can still initiate; (iii) extrapolation of strength data from the macroscale to the nanoscale is not valid; and (iv) most importantly, silicon is uncommonly brittle and susceptible to strength loss in the subthreshold region of nanoscale flaws.

ACKNOWLEDGMENTS

The authors thank Douglas Smith for assistance with the nanoindentation experiments and Yan Deng for taking the AFM micrographs in Figs. 1 and 2. This work was sponsored by NIST internal funds; by a grant from the Junta de Extremadura-Consejeria de Educacion Ciencia y Tecnologia y el Fondo Social Europeo, Spain (Grant IPR00A084); by Secretaria de Estado de Educacion y Universidades, Spain (A.P.); and by a NIST/NSF Summer Undergraduate Research Fellowship (M.C.).

Information of product names and suppliers in this paper is not to imply endorsement by NIST.

REFERENCES

1. B. Bushan, *Tribology and Mechanics of Magnetic Storage Devices*, Second ed. (Springer-Verlag, New York, 1996).
2. H. Kahn, N. Tayebi, R. Ballarini, R.L. Mullen, and A.H. Heuer, Sens. Actuators A **82,** 274 (2000).
3. T. Namazu, Y. Isono, and T. Tanaka, Journal of Microelectromechanical Systems **9,** 450 (2000).
4. J.N. Ding, Y.G. Meng, and S.Z. Wen, J. Mater. Res. **16,** 2223 (2001).
5. R.D. Maurer, in *Strength of Inorganic Glass*, edited by C.R. Kurkjian (Plenum Press, New York, 1985), pp. 291–308.
6. B.R. Lawn, *Fracture of Brittle Solids*, Second ed. (Cambridge University Press, Cambridge, 1993), Ch. 8.
7. T.P. Dabbs, D.B. Marshall, and B.R. Lawn, J. Am. Ceram. Soc. **63,** 224 (1980).
8. T.P. Dabbs and B.R. Lawn, Phys. Chem. Glasses **23,** 93 (1982).
9. T.P. Dabbs and B.R. Lawn, J. Am. Ceram. Soc. **68,** 563 (1985).
10. K. Jakus, J.E. Ritter, S.R. Choi, T. Lardner, and B.R. Lawn, J. Non-Cryst. Solids **102,** 82 (1988).
11. B. Lin and M.J. Matthewson, Philos. Mag. A **74,** 1235 (1996).
12. H. Chai, B.R. Lawn, and S. Wuttiphan, J. Mater. Res. **14,** 3805 (1999).
13. Y-W. Rhee, H-W. Kim, Y. Deng, and B.R. Lawn, J. Am. Ceram. Soc. **84,** 1066 (2001).
14. P. Miranda, A. Pajares, F. Guiberteau, F.L. Cumbrera, and B.R. Lawn, Acta Mater. **49,** 3719 (2001).
15. P. Miranda, A. Pajares, F. Guiberteau, Y. Deng, and B.R. Lawn, Acta Mater. **51,** 4347 (2003).
16. B.R. Lawn, D.B. Marshall, and P. Chantikul, J. Mater. Sci. **16,** 1769 (1981).
17. D.B. Marshall, B.R. Lawn, and P. Chantikul, J. Mater. Sci. **14,** 2225 (1979).
18. R.F. Cook and D.H. Roach, J. Mater. Res. **1,** 589 (1986).
19. S. Lathabai, J. Rödel, B.R. Lawn, and T.P. Dabbs, J. Mater. Sci. **26,** 2157 (1991).
20. M.V. Swain and J.T. Hagan, J. Phys. D: Appl. Phys. **9,** 2201 (1976).
21. J.T. Hagan and M.V. Swain, J. Phys. D **11,** 2091 (1978).
22. J.T. Hagan, J. Mater. Sci. **15,** 1417 (1980).
23. B.R. Lawn, T.P. Dabbs, and C.J. Fairbanks, J. Mater. Sci. **18,** 2785 (1983).
24. B.R. Lawn, A.G. Evans, and D.B. Marshall, J. Am. Ceram. Soc. **63,** 574 (1980).
25. J.G. Bradby, J.S. Williams, J. Wong-Leung, M.V. Swain, and P. Munroe, J. Mater. Res. **16,** 1500 (2001).
26. J.G. Bradby, J.S. Williams, J. Wong-Leung, S.O. Kucheyev, M.V. Swain, and P. Munroe, Philos. Mag. A **82,** 1931 (2002).
27. I. Zarudi, L.C. Zhang, and M.V. Swain, J. Mater. Res. **18,** 758 (2003).
28. B.R. Lawn and D.B. Marshall, J. Am. Ceram. Soc. **62,** 347 (1979).